

Effects of diffusion boundary layer on reaction kinetics of immunoassay in a biosensor

Chih-Kai Yang, Jeng-Shian Chang,^{a)} Sheng D. Chao,^{b)} and Kuang-Chong Wu
Institute of Applied Mechanics, National Taiwan University, Taipei 106, Taiwan

(Received 28 June 2007; accepted 27 February 2008; published online 28 April 2008)

Specific binding reaction is a natural characteristic that is applied to design biosensors. This work simulates the binding reaction kinetics of two commonly used proteins, C-reactive protein and immunoglobulin G, in a reaction chamber (microchannel) of a biosensor. For a diffusion-limited protein, the diffusion boundary layer on the reaction surface of the biosensor would hinder the binding reaction from association and dissociation. Several crucial factors, which influence the binding reaction curves in the simulation, are discussed, including the concentration of analyte, the inlet flow velocity, the channel height, and the length of the reaction surface. A higher channel causes the diffusive transport of the analyte to take longer time to reach the reaction surface, which in turn decreases the reaction rate of the protein pairs. The length of the reaction surface plays an important role in the formation of the boundary layer. For longer reaction surface, it takes more time to allow diffusion to overcome the larger zone of the diffusion boundary layer, resulting in a slower binding rate and a longer time to reach saturation. The presented data of simulation are useful in designing the biosensors. © 2008 American Institute of Physics. [DOI: 10.1063/1.2909980]

I. INTRODUCTION

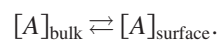
In recent years, the study of biosensors has become an active research field. It brings many interesting applications of nanotechnology to the area of biochemical and biological systems. The development of immunoassay places special emphasis on the high sensitivity and real-time detecting ability for various biosensors. The three most commonly used devices in detecting biomolecules are the microcantilever-based biosensor, the surface plasmon resonance (SPR) sensor, and the quartz crystal microbalance (QCM) sensor. Although the basic principles of detection for these sensors are different, they all involve the same kinetics of specific recognition of analytes and immobilized ligands, in which the concentration of the binding complex of analytes and ligands on the reaction surface plays a key role.

It is important to monitor the patient who suffers from a high risk epidemic such as cardiovascular disease. Human C-reactive protein (CRP), first discovered in 1930,¹ is a typical acute-phase protein as a clinical indicator of many inflammatory conditions. CRP is usually present in human serum with a concentration $<1 \mu\text{g/ml}$. However, CRP concentration level can increase up to tens or even hundreds times when the inflammation occurs. Human CRP is a homogeneous protein (molecular weight of $\sim 115 \text{ kDa}$) which consists of five identical noncovalently bonded monomer subunits (molecular weight of $\sim 23 \text{ kDa}$) linking in the form of a cyclic pentamer. In an immunoassay experiment, the common protein pair of antigen and antibody is human CRP and its monoclonal antihuman CRP. It is known that diffusion and binding ability are important factors in the reaction kinetics. These two factors diversely differ for different protein pairs. Thus for the purpose of comparison, not only the

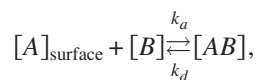
protein pair of human CRP and antihuman CRP but another common protein pair of mouse Immunoglobulin G (IgG) and antimouse IgG are simulated for the study of stoichiometry in this work.

The specific recognition of analytes and immobilized ligands occurs at the reaction surface of a biosensor, which is a solid-liquid interface. The reaction kinetics can be described as a two-step process.²

- (1) Mass-transport process: The analyte is transported by diffusion from the bulk solution toward the reaction surface.



- (2) Chemical reaction process: The binding of the protein pair takes place.



where $[A]_{\text{bulk}}$ is the concentration of the analyte in the bulk, $[A]_{\text{surface}}$ is the analyte concentration at the reaction surface, $[B]$ is the ligand concentration, $[AB]$ is the analyte-ligand complex concentration, k_a is the association rate constant, and k_d is the dissociation rate constant.

When the analyte takes a longer time to transport (by convection and diffusion) to the reaction surface than chemical reaction, the whole reaction is restrained by mass-transport process. This usually causes the formation of a diffusion boundary layer.³ For the biosensors operating in fluid environment, the diffusion velocity of many biomolecules is relatively slow compared to the reaction velocity, as measured by the Damkoehler number.⁴ Thus on the reaction surface, where the flow is static under the assumption of nonslip flow condition, the diffusion boundary is formed. The size of the zone of the diffusion boundary layer depends on the ratio

^{a)}Electronic mail: jschang@spring.iam.ntu.edu.tw.

^{b)}Electronic mail: sdchao@spring.iam.ntu.edu.tw.

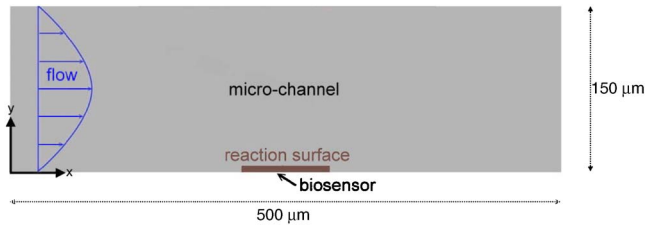


FIG. 1. (Color online) Sketch of the 2D model. The size of the biosensor is $40\ \mu\text{m}$ in length and $3\ \mu\text{m}$ in thickness. The channel size is $500\ \mu\text{m}$ in length and $150\ \mu\text{m}$ in height.

of reaction rate to the diffusion rate and the flow velocity adjacent to the reaction surface.⁵ Besides, the size of the diffusion boundary layer will grow along the reaction surface in the flow direction. As the whole reaction (association or dissociation) is complete, the diffusion boundary layer will disappear. Thus the size of the diffusion boundary layer is a good measure of reaction velocity.

In this paper we simulate two dimensional (2D) full time scale processes of association and dissociation in a biosensor immunoassay with the samples of CRP pairs and IgG pairs, using the finite element analysis software, COMSOL MULTIPHYSICS™.⁶ Calculations of the surface concentration of the analyte-ligand complex versus time during the entire biochemical reaction are performed to study the effects of several related parameters on the detection of biomolecules with the biosensor. The plan of the paper is as follows. In Sec. II, the equations governing the flow field, the concentration field, and the biochemical reaction are described. Detailed geometry, flow properties, diffusion constant, and binding constants, initial and boundary conditions that are required for simulation are described in Sec. III. Numerical calculations are then performed to solve the velocity field of the fluid flow, the concentration field of the analyte, in the bulk, the surface concentration of the analyte and the surface concentration of the analyte-ligand complex. Finally the results are presented in Sec. IV. As for the biosensor with a narrower reaction surface, such as a microcantilever beam sensor, 2D simulations could show large deviation from three dimensional (3D) simulations. In Sec. IV F, we will demonstrate the difference of the binding reaction curves based on the 3D simulations and the 2D simulations for the reaction surface with various aspect ratios (length to width).

II. THEORY

Consider a 2D model of a biosensor in a microchannel, as shown in Fig. 1. The dimension of the biosensor is $40\ \mu\text{m}$ in length and $3\ \mu\text{m}$ in thickness and that of the microchannel is $500\ \mu\text{m}$ in length and $150\ \mu\text{m}$ in height. It is assumed that the reaction surface has the same length as that of the biosensor. The x -axis is set to be along the flow direction and y -axis is the direction of the channel height. The left corner of the bottom side is chosen as the origin. The buffer solution mixed with the analyte flows from the left to the right along the x -direction. On the reaction surface ($230 \leq x \leq 270, y = 3$) of the biosensor are the immobilized ligands. The center of the biosensor is located in the middle of the bottom side, $(250, 1.5)$, where the unit is micrometers. Notice that the

length of the biosensor and the height of the microchannel will be altered in Sec. IV to discuss the geometry effects on the enhancement of the association and dissociation kinetics. The equations governing the flow field, the concentration field, and the biochemical reaction are given below.

A. The flow field

In this work it is assumed that the fluid is incompressible so that

$$\frac{\partial u}{\partial x} + \frac{\partial v}{\partial y} = 0, \quad (1)$$

where u and v are, respectively, the x and the y velocity components. The equations of motion are as follows:

$$\rho \frac{\partial u}{\partial t} + \rho \left(u \frac{\partial u}{\partial x} + v \frac{\partial u}{\partial y} \right) - \eta \nabla^2 u + \frac{\partial p}{\partial x} = 0, \quad (2)$$

$$\rho \frac{\partial v}{\partial t} + \rho \left(u \frac{\partial v}{\partial x} + v \frac{\partial v}{\partial y} \right) - \eta \nabla^2 v + \frac{\partial p}{\partial y} = 0, \quad (3)$$

where η is the dynamic viscosity of fluid, ρ is the density of fluid, and p is the pressure, respectively. In this work, it is assumed that the density ρ and viscosity η of the modeled incompressible fluid are constant independent of the temperature and the concentration.

B. The concentration field

Transport of analytes to and from the surface is assumed to be described by the Fick second law with convective terms:

$$\frac{\partial [A]}{\partial t} + u \frac{\partial [A]}{\partial x} + v \frac{\partial [A]}{\partial y} = D \left(\frac{\partial^2 [A]}{\partial x^2} + \frac{\partial^2 [A]}{\partial y^2} \right), \quad (4)$$

where $[A]$ ($= [A]_{\text{bulk}}$) is the bulk concentration of analyte and D is the diffusion coefficient of analyte.

C. The reaction surface

The reaction between immobilized ligand and analyte is assumed to follow the first order Langmuir adsorption model.^{3,7} During the reaction, the concentration of the analyte-ligand complex $[AB]$ increases as a function of time according to the reaction rate equation

$$\frac{\partial [AB]}{\partial t} = k_a [A]_{\text{surface}} \{ [B_0] - [AB] \} - k_d [AB], \quad (5)$$

where $[A]_{\text{surface}}$ is the concentration of the analyte at the reaction surface by mass transport, $[B_0]$ is the initial surface concentration of the ligand, $[AB]$ is the surface concentration of the analyte-ligand complex, k_a is the association rate constant, and k_d is the dissociation rate constant.

III. SIMULATION DETAILS

An unstructured mesh consisting of triangular elements is generated for the calculation. Figure 2 shows this mesh where the region near the biosensor is refined for a better resolution.

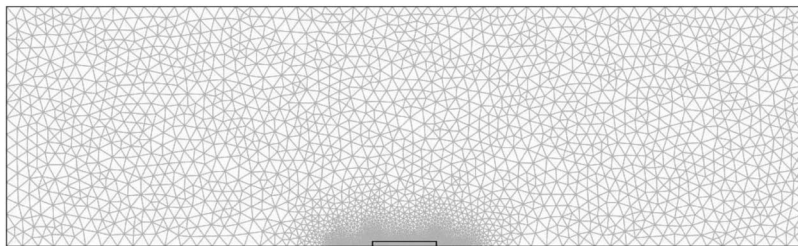


FIG. 2. 2D unstructured mesh with triangular elements.

A. The flow field configuration

In an immunoassay experiment, phosphate buffer saline (PBS) is usually used to be a neutral buffer solution ($pH = 7.2$), which is mixed with analytes as a carrier fluid. The physical properties of such a fluid are similar to water. The dynamic viscosity η is 10^{-3} Pa s. Since the flow in the microchannel is in a low Reynolds number condition, it is assumed to be a laminar flow. The average velocity of the parabolic profile is set as $u = 10^{-4}$ m/s at the inlet of the microchannel. Boundary conditions are $p = 0$ at the outlet, and nonslip elsewhere. The fluid is assumed to be at rest initially. The flow field can be determined by solving Eqs. (1)–(3) in conjunction with the boundary and initial conditions.

B. The concentration field configuration and kinetics of the specific binding

The diffusion coefficients of human CRP are taken as 2.175×10^{-11} m²/s and that of IgG as 5×10^{-11} m²/s.^{8,9} Five inlet concentrations of the analyte $[A]$, 0.64, 1.92, 6.4, 19.2, and 64 nM, are considered. The initial surface concentration $[B_0]$ of the immobilized ligand is assumed as 1.4×10^{-8} mole/m².¹⁰ At the reaction surface, the diffusive flux is balanced against the reaction rate

$$-D \left(\frac{\partial [A]}{\partial y} \right)_{\text{surface}} = k_a [A]_{\text{surface}} \{ [B_0] - [AB] \} - k_d [AB]. \quad (6)$$

The association rate constant k_a and the dissociation rate constant k_d of the protein pairs can be found in Ref. 11. The values of k_a and k_d for CRP-anti-CRP binding interactions are 1.0×10^7 M⁻¹ s⁻¹ and 2.6×10^{-2} s⁻¹, respectively. The values of k_a and k_d for IgG-anti-IgG binding interactions are 2.5×10^5 M⁻¹ s⁻¹ and 3×10^{-4} s⁻¹, respectively.

The initial conditions for both the concentration of the analyte in the bulk, $[A]$, and the concentration of the analyte-ligand complex on the reaction surface, $[AB]$, are all zero.

Once the flow field is determined, Eqs. (4) and (5) can be solved with the initial and boundary conditions described above to yield $[A]_{\text{bulk}}$, $[A]_{\text{surface}}$, and $[AB]$ versus time during the entire reaction. In particular, the area average of $[AB]$ over the reaction surface is performed and presented in the simulation results below.

The dissociation phase of the binding reaction of the two protein pairs is simulated by terminating the supply of the analyte at a time after the binding reaction is saturated.

It is noted in our examples that the association reaction rates ($k_a [B_0]$) for CRP and IgG in the PBS solution are,

respectively, 140 and $3.5 \mu\text{m/s}$. The diffusion rates (D/h) for CRP molecule and IgG in the PBS solution are, respectively, 0.14 and $0.33 \mu\text{m/s}$ when h is picked as $150 \mu\text{m}$. Since on the reaction surface the association rate is faster than the diffusion rate for both CRP and IgG, the diffusion boundary layer will form during the binding reaction.

IV. RESULTS

We have performed the 2D finite element simulations to evaluate the binding curves during the association and dissociation and presented the results in Secs. IV A–IV E. The results are examined to be mesh independent by means of a convergence test. Effects of some crucial parameters are also discussed in this section. It is expected that for the reaction surface having small aspect ratio (length to width), namely, wider reaction surface, the 2D simulation should be accurate enough. However, for the system with relatively narrower reaction surface, 3D calculations are expected to be required. This is discussed in Sec. IV F

A. Binding kinetics of CRP and IgG

The simulated binding reaction curves for CRP and IgG are shown in Figs. 3 and 4, respectively, corresponding to the different concentrations of the analyte, namely, 0.64, 1.92, 6.4, 19.2, and 64 nM. Although the dissociation equilibrium constants K_D of the two proteins CRP and IgG are comparable as medium affinity (CRP: $2.6 \times 10^{-9} M$, IgG: $1.2 \times 10^{-9} M$), the characteristic behaviors in the association phase or the dissociation phase are different. The response of CRP is apparently faster than that of IgG. The main reason is that both values of k_a and k_d of CRP are greater than those of IgG.

The analyte concentration $[A]$ versus the complex concentration $[AB]_{\text{sat}}$ can be obtained through Eq. (5) by requiring $\partial [AB] / \partial t = 0$ (i.e., at the equilibrium of the association):

$$[A] \approx [A]_{\text{surface}} = \frac{k_d / k_a}{[B_0] / [AB]_{\text{sat}} - 1} = \frac{K_D}{[B_0] / [AB]_{\text{sat}} - 1}, \quad (7)$$

where $K_D \equiv k_d / k_a$ is the dissociation equilibrium constant. Equation (7) is plotted in Fig. 5, in which the squares denote the simulated data ($[A], [AB]_{\text{sat}}$) picked from Figs. 3 and 4. Consistency of the simulated data with Eq. (7) serves to demonstrate the correctness of our simulation.

Equation (7) is not convenient to use from the experimental point of view since the measured response R of a biosensor, such as QCM or SPR, is not the concentration of the analyte-ligand complex itself but rather a quantity that is assumed to be proportional to the concentration of the analyte-ligand complex (i.e., $R = \alpha [AB]$, where α is a con-

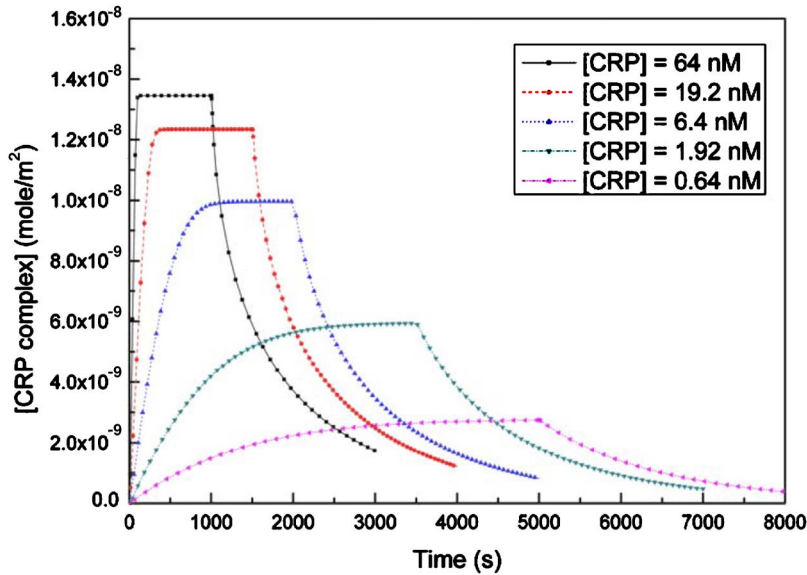


FIG. 3. (Color online) The average surface concentration of CRP-anti-CRP complex along the surface as a function of time for different CRP bulk concentrations.

stant). Thus a simple revision of Eq. (7) is desirable. In the experiment with a very dense concentration of the analyte $[\hat{A}]$ such that $K_D/[\hat{A}] \ll 1$, the initial concentration $[B_0]$ of the ligand can be obtained as the maximum equilibrium response \hat{R}_{eq} divided by the constant α :

$$[B_0] = [\hat{A}\hat{B}]_{sat} \left(1 + \frac{K_D}{[\hat{A}]_{surface}} \right) \approx [\hat{A}\hat{B}]_{sat} \left(1 + \frac{K_D}{[\hat{A}]} \right) \approx [\hat{A}\hat{B}]_{sat} = \hat{R}_{eq}/\alpha, \quad (8)$$

where $[\hat{A}\hat{B}]_{sat}$ is the maximum concentration of the analyte-ligand complex. When $[B_0]$ is known, K_D can be estimated as

$$K_D \approx [A]^* (\hat{R}_{eq}/R_{eq}^* - 1), \quad (9)$$

where R_{eq}^* is the response at equilibrium in an experiment, in which the concentration of the analyte is $[A]^*$. Finally, the relationship $[A]$ versus R_{eq} is given as

$$[A] \approx \frac{K_D}{\hat{R}_{eq}/R_{eq} - 1}. \quad (10)$$

In other words, by conducting only two experiments, one with very dense concentration of the analyte and the other one with a medium concentration of the analyte, one can determine \hat{R}_{eq} and K_D . Thus the concentration $[A]$ of the analyte in the follow-up experiments can be predicted according to Eq. (10) when the response of the association at equilibrium is measured.

B. The diffusion boundary layer

Under the assumption of nonslip flow boundary condition, the consumption of $[A]_{surface}$ in the association phase is faster than the supply from the bulk on the reaction surface, if the diffusion rate of analyte is slower than the reaction rate. Thus a small diffusion boundary layer of the analyte is formed near the reaction surface. Within the boundary layer, there is a shortage of the analyte. The diffusion boundary

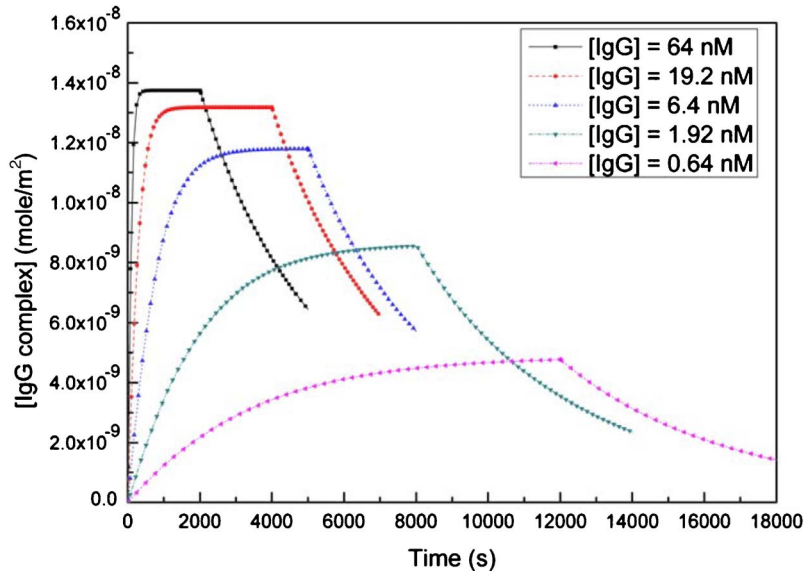


FIG. 4. (Color online) The average surface concentration of IgG-anti-IgG complex along the surface as a function of time for different IgG bulk concentrations.

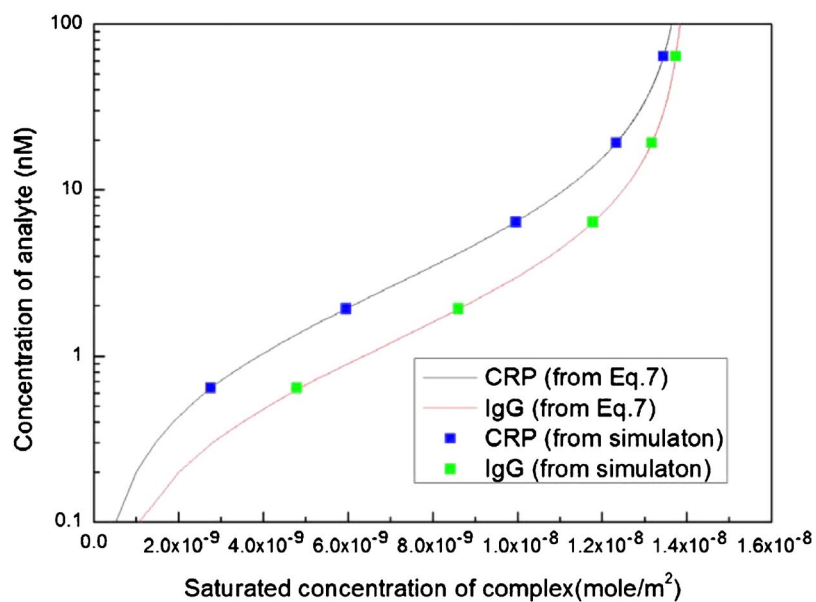


FIG. 5. (Color online) The saturated concentration of analyte-ligand complex as a function of the concentration of analyte in the bulk.

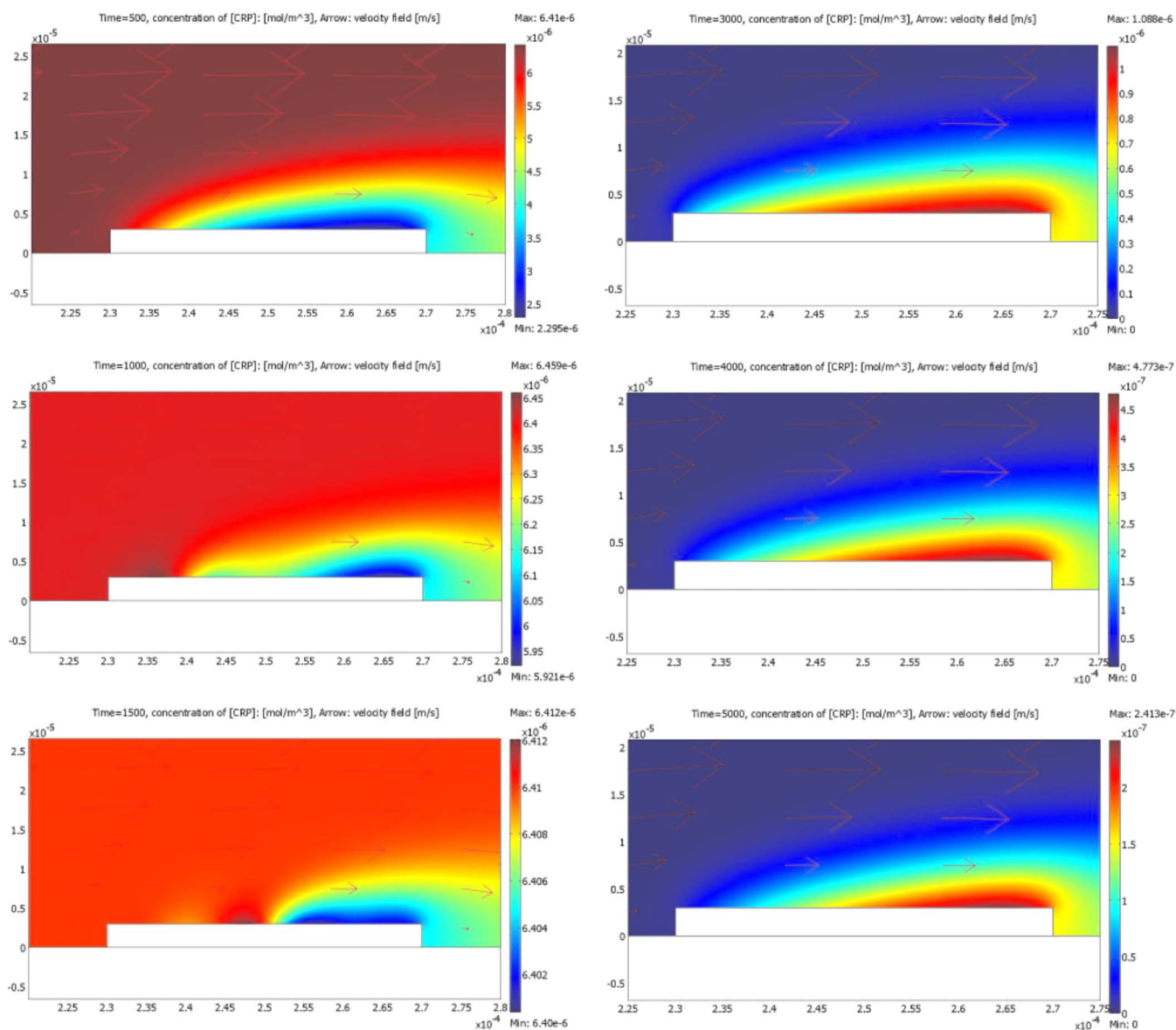


FIG. 6. (Color online) The development of the diffusion boundary layer of the CRP binding reaction. The biosensor is located at (250, 1.5) and the concentration of CRP is 6.4 nM. The left three illustrations are in association phase at times of 500, 1000, and 1500 s, and the right three illustrations are in dissociation phase at times of 3000, 4000, and 5000 s. Notice that the density scales are different to increase the plot visibility.

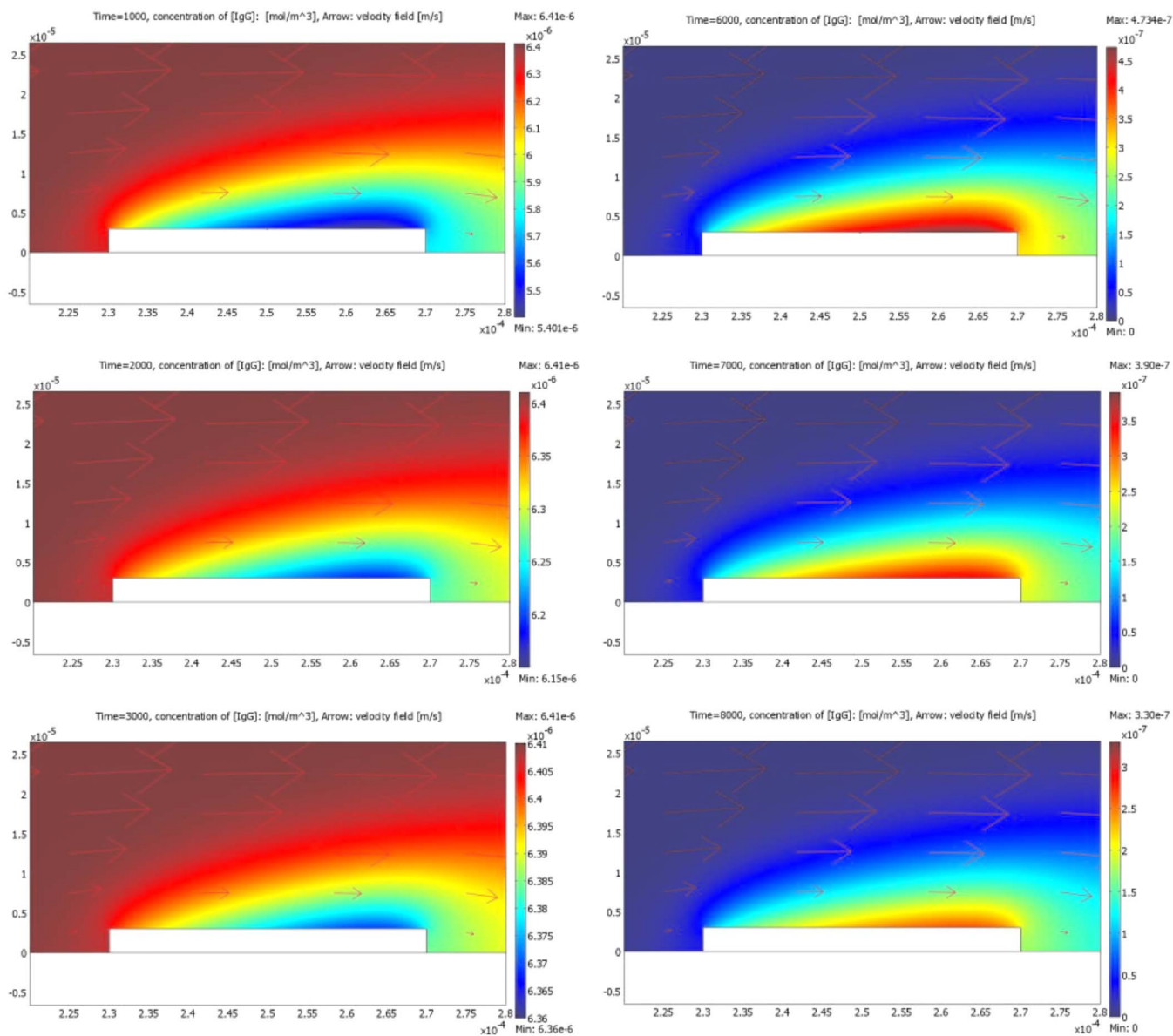


FIG. 7. (Color online) The development of the diffusion boundary layer of the IgG binding reaction. The biosensor is located at (250, 1.5) and the inlet concentration of IgG is 6.4 nM. The left three illustrations are in association phase at times of 1000, 2000, and 3000 s, and the right three illustrations are in dissociation phase at times 6000, 7000, and 8000 s. Notice that the density scales are different to increase the plot visibility.

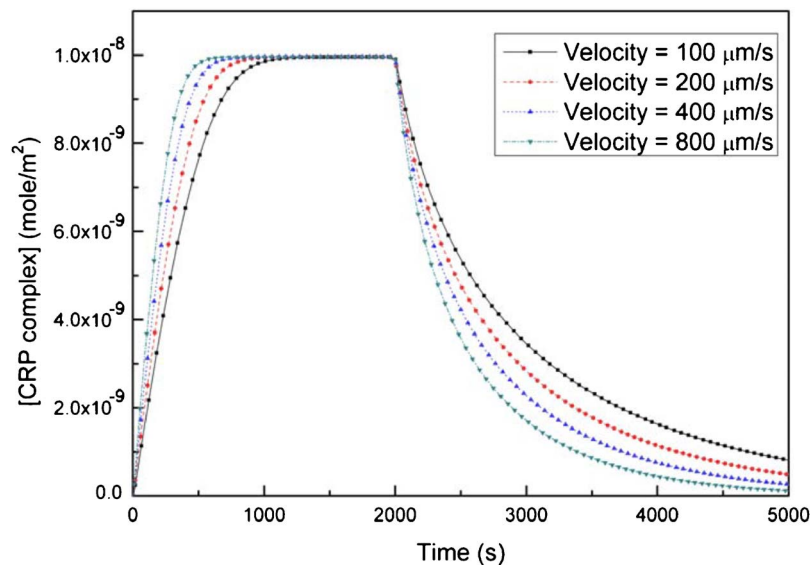


FIG. 8. (Color online) Influence of raising the inlet flow velocity on the curve of the surface concentration of CRP complex vs. time. Notice that the biosensor is located at (250, 1.5) and the inlet concentration of CRP is 6.4 nM.

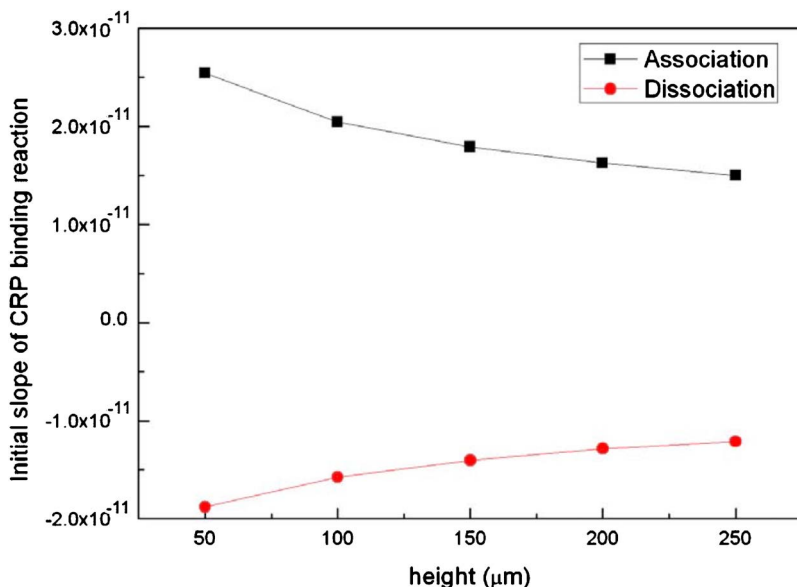


FIG. 9. (Color online) The initial slope of CRP binding reaction as a function of channel's height. The inlet concentration of CRP is 6.4 nM. The channel's inlet flow velocity is 100 $\mu\text{m/s}$.

layer also occurs in the dissociation phase when the supply of analyte in the flow is terminated. In the latter case the situation is reversed; namely, within the boundary layer, there is a denser concentration of the analyte than that in the bulk. Figures 6 and 7 show the time evolutions of the diffusion boundary layers of the CRP and IgG protein pairs, respectively, from the association phase (the left panels) to the dissociation phase (the right panels). Notice that the density scales are different to increase the plot visibility. With a continuous supply of the analyte, the boundary layer is progressively eliminated during the association phase. Similarly, the boundary layer also gradually vanishes in the dissociation phase due to the termination of the supply of the analyte in the bulk. Obviously, any means to limit the growth of this boundary layer will raise the rates of the association and dissociation, as will be discussed in the next few subsections.

C. Effect of inlet flow velocity

Raising flow velocity is an effective means to reduce the thickness of the diffusion boundary layer. Figure 8 presents

the effect of raising the inlet flow velocity on the CRP-anti-CRP binding kinetics. As expected, the faster the inlet flow velocity is, the faster association and dissociation rates are.

D. Effect of height of the reaction channel

In this subsection the height of the reaction channel is allowed to vary. It is also noted that in each case of various channel heights, the flow rate is different but the average velocity ($=100 \mu\text{m/s}$) through the channel cross sections remains the same. In addition, the center of the biosensor is set at the position (250, 1.5) with the inlet analyte concentration of 6.4 nM. Figures 9 and 10 show the initial slopes of the binding curves for average surface concentration of the CRP complex and IgG complex along the surface, respectively. The height of the channel varies from 50 to 250 μm . Larger slopes are found for lower channel height for both CRP and IgG protein pairs. This can be understood as faster diffusion in transporting the analytes for the channel with a lower height.

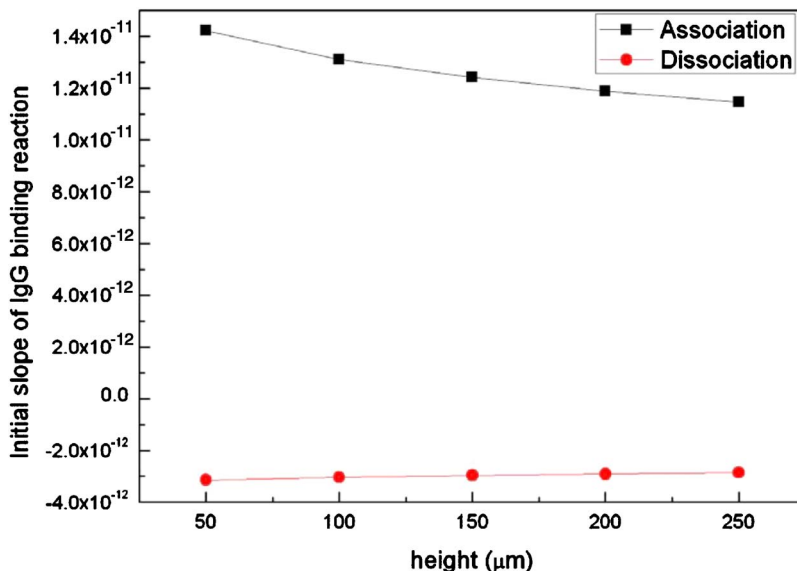


FIG. 10. (Color online) The initial slope of IgG binding reaction as a function of channel's height. The inlet concentration of IgG is 6.4 nM. The channel's inlet flow velocity is 100 $\mu\text{m/s}$.

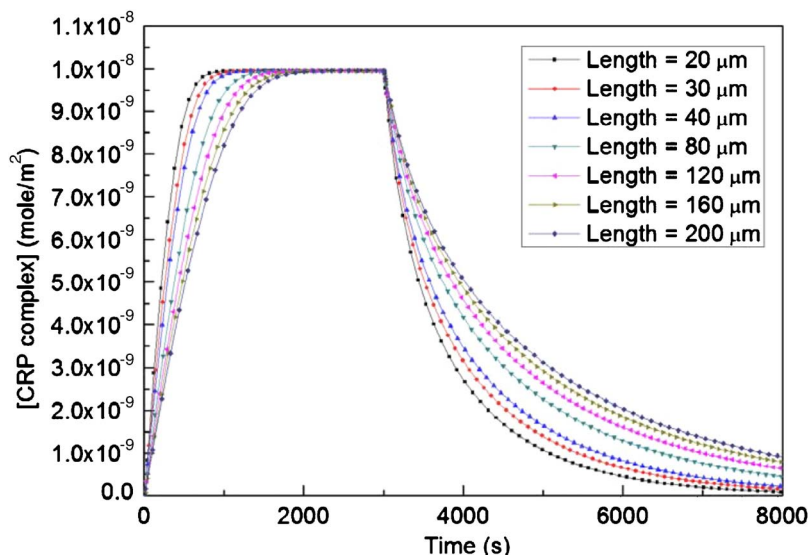


FIG. 11. (Color online) The average surface concentration of CRP complex along the surface as a function of time for various lengths of the reaction surface. The concentration of CRP is 6.4 nM. The channel's inlet flow velocity is 100 $\mu\text{m/s}$. The size of the channel is shown in Fig. 1.

E. Effect of the length of the reaction surface

To study the effect of the length of the reaction surface on the reaction rates, we vary the length of the reaction surface from 20 to 200 μm . The inlet concentration of the analyte is constant ($=6.4$ nM), and the supply of the analyte is sustained for 3000 s. The binding reaction curves for CRP are shown in Fig. 11, and the formation of the diffusion boundary layer on the reaction surface at time=500 s is shown in Fig. 12. As expected, the required time to reach a steady state gets longer when the span of the boundary layer is longer. The results for IgG are similar to those for CRP and are not shown here. Although shortening the length of the reaction surface could restrain the expansion of the boundary layer, the detecting techniques of a biosensor may require a sufficiently long reaction surface to satisfy its limit of detection. Consequently, some kind of compensation should be considered in the biosensor design.

F. Effect of width: 3D simulation

In some biosensors, the reaction surface may occupy the whole or half of the bottom surface of the microchannel such

as SPR and QCM. As for the microcantilever beam sensor, the size of reaction surface, especially the width, is rather small compared to that of the microchannel. Thus it is appropriate to compare the difference between the binding curve predicted by 2D simulation and that by 3D simulation.

Figure 13 shows the sketch of a 500 μm (length) \times 500 μm (width) \times 150 μm (height) microchannel with a biosensor put on the middle of the bottom surface. There are four sizes of biosensor chosen to perform 3D simulation, namely, 40 \times 500 \times 3 μm^3 , 40 \times 200 \times 3 μm^3 , 40 \times 50 \times 3 μm^3 , and 40 \times 20 \times 3 μm^3 . Results of 3D simulation together with that of 2D simulation (the sensor with 40 μm in length and 3 μm in height) for the average concentration of CRP complex along the length direction of the biosensor are shown in Fig. 14, where the average inlet flow velocity of 100 $\mu\text{m/s}$ and the inlet bulk concentration of CRP of 6.4 nM are used. It is seen that the binding curve of the biosensor of width 500 μm , which is the same as the width of the microchannel, predicted by 3D simulation is virtually the same as that predicted by 2D simulation. Besides, it is the trend that 3D simulation yields the faster binding reaction than 2D

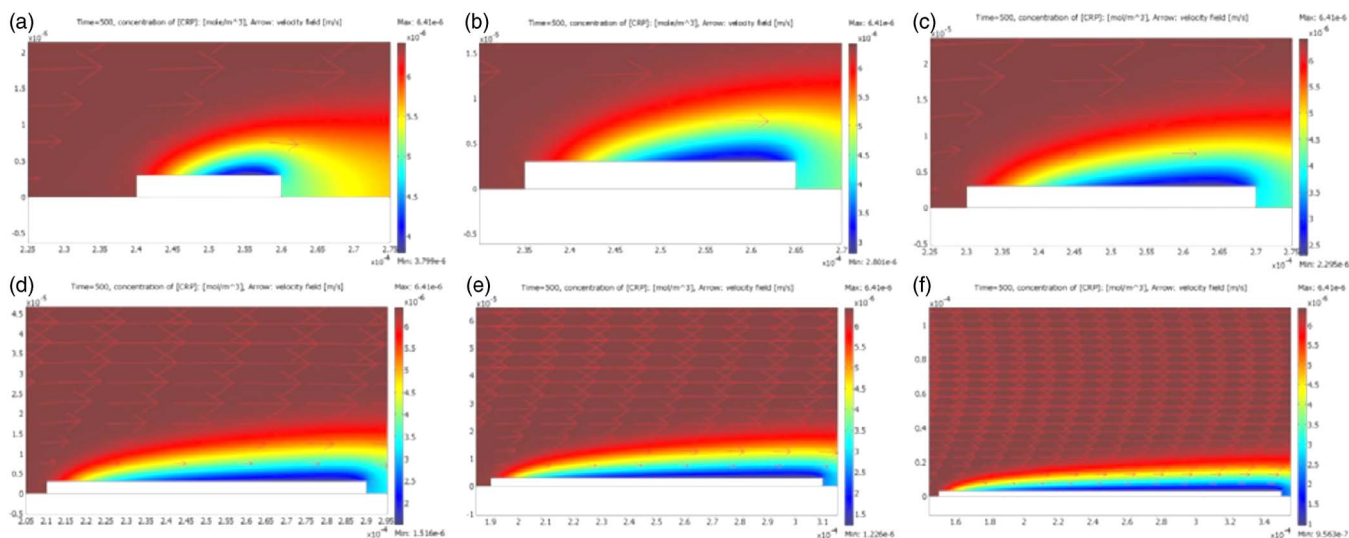


FIG. 12. (Color online) The expansion of the diffusion boundary layer for varying lengths of the reaction surface. It is noticed that the time=500 s for (a) 20 μm , (b) 30 μm , (c) 40 μm , (d) 80 μm , (e) 120 μm , and (f) 200 μm , respectively.

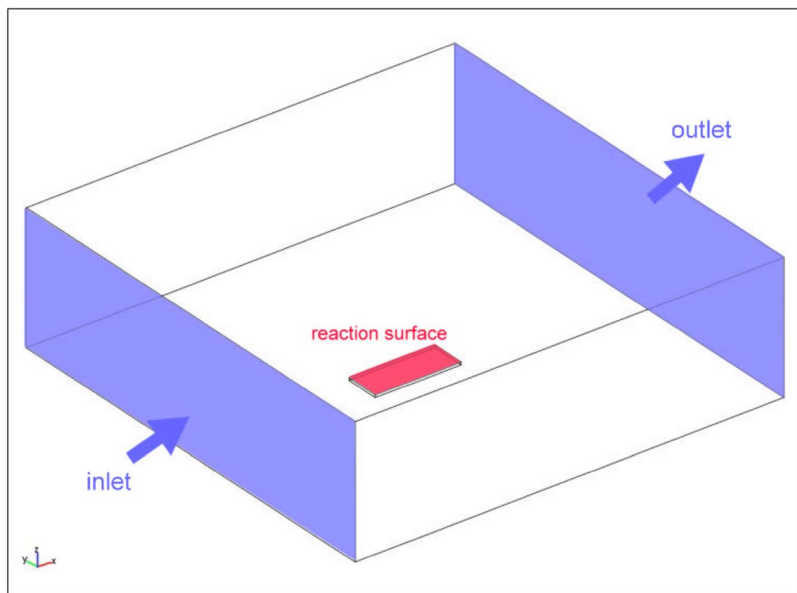


FIG. 13. (Color online) Sketch of the 3D model. The channel size is $500\ \mu\text{m}$ in length, $500\ \mu\text{m}$ in width, and $150\ \mu\text{m}$ in height. The biosensor, $40\ \mu\text{m}$ in length, $3\ \mu\text{m}$ in height, and variable width, is put on the center of the bottom surface.

simulation does as the width of the biosensor gets smaller. Hence, it is suggested that 3D simulation is necessary for high aspect ratio (ratio of length to width) biosensor to yield more accurate prediction and that the biosensor with high aspect ratio will have better performance.

V. CONCLUSION

This paper presents 2D numerical simulations on the immunoassay in a biosensor by using the finite element analysis software, COMSOL MULTIPHYSICS™. Two commonly used proteins, CRP and IgG, are used as the analytes for the analysis of the binding kinetics.

The existence of the diffusion boundary layer restrains the association and dissociation reaction rates for the slow diffusion protein pairs and nonslip flow boundary condition, which affects the performance of the biosensors. Several crucial factors have been discussed, namely, the concentration of the analyte, the inlet flow velocity, the height of the

channel, and the length of the reaction surface. It is expected that the denser concentration of the analyte yields the faster association and dissociation rates. Raising flow velocity can effectively reduce the thickness of the diffusion boundary layer. A lower channel causes the diffusion to take less time to transport the analyte to the reaction surface and hence increases the association and dissociation rates of the protein pairs. Moreover, the shorter the reaction surface along the flow direction is, the smaller the diffusion boundary layer is. Thus shortening the length of the reaction surface can also raise both the association and dissociation rates. In summary, the faster inlet flow velocity, the lower channel, and the shorter reacting surface can reduce the growth of the diffusion boundary layer and raise the performance of the biosensor. Finally, if the width of the biosensor is relatively small compared to that of the microchannel, 3D simulations are necessary to predict more accurate results. These results presented in this work should be very useful for designing biosensors.

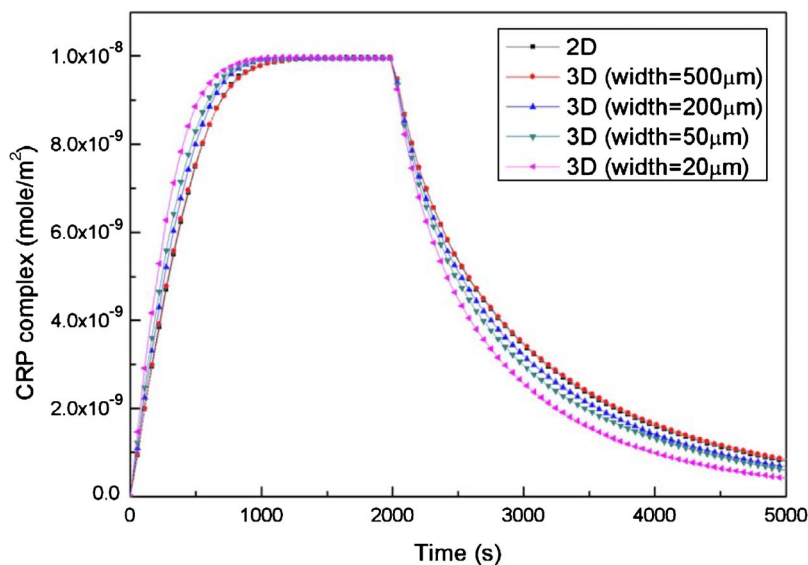


FIG. 14. (Color online) The average surface concentration of CRP-anti-CRP complex along the surface as a function of time for the reaction surface with various widths.

ACKNOWLEDGMENTS

This research was supported by the National Science Council in Taiwan through NSC 96-2120-M-002-014. We thank the NCHC for providing computing resources.

¹W. S. Tillet and T. Francis, *J. Exp. Med.* **52**, 561 (1930).

²N. Camillone, *Langmuir* **20**, 1199 (2004).

³D. B. Hibbert and J. J. Gooding, *Langmuir* **18**, 1770 (2002).

⁴W. M. Deen, *Analysis of Transport Phenomena* (Oxford University Press,

New York, 1998).

⁵C. K. Yang, J. S. Chang, S. D. Chao, and K. C. Wu, *Appl. Phys. Lett.* **91**, 113904 (2007).

⁶COMSOL MULTIPHYSICS, Version 3.3, COMSOL Ltd., Stockholm, Sweden.

⁷I. Langmuir, *J. Am. Chem. Soc.* **40**, 1361 (1918).

⁸Y. Hokama, M. K. Coleman, and R. F. Riley, *J. Immunol.* **95**, 156 (1965).

⁹H. A. Leddy and F. Guilak, *Ann. Biomed. Eng.* **31**, 753 (2003).

¹⁰E. Behraves, V. I. Sikavitsas, and A. G. Mikos, *Biomaterials* **24**, 4365 (2003).

¹¹C. Chou, H. Y. Hsu, H. T. Wu, K. Y. Tseng, A. Chiou, C. J. Yu, Z. Y. Lee, and T. S. Chan, *J. Biomed. Opt.* **12**, 0240251 (2007).